Nina Gaiser, Thomas Bierkandt, Patrick Oßwald, Julia Zinsmeister, Trupti Kathrotia, Shkelqim Shaqiri, Patrick Hemberger, Tina Kasper, Manfred Aigner, Markus Köhler, Oxidation of oxymethylene ether (OME0-5): An experimental systematic study by mass spectrometry and photoelectron photoion coincidence spectroscopy, Fuel 313 (2022) 122650.

The original publication is available at www.elsevier.com

https://doi.org/10.1016/j.fuel.2021.122650

Oxidation of oxymethylene ether (OME_{0-5}): An experimental systematic study by mass spectrometry and photoelectron photoion coincidence spectroscopy

Nina Gaiser[1*], Thomas Bierkandt[1], Patrick Oßwald[1], Julia Zinsmeister[1], Trupti Kathrotia[1], Shkelqim Shaqiri[2], Patrick Hemberger[3], Tina Kasper[2], Manfred Aigner[1], Markus Köhler[1]

[1]Institute of Combustion Technology, German Aerospace Center (DLR), Stuttgart, Germany
[2]Mass Spectrometry in Reactive Flows, IVG, University of Duisburg-Essen, Duisburg, Germany
[3]Laboratory for Synchrotron Radiation and Femtochemistry, Paul Scherrer Institute, Villigen, Switzerland

*Corresponding Author: Nina Gaiser,
German Aerospace Center, Pfaffenwaldring 38-40,
70569 Stuttgart, Germany
Phone: +49-711-6862-378
E-mail: nina.gaiser@dlr.de

Abstract

This paper presents a systematic study of oxymethylene ethers (OMEs) oxidation in an atmospheric laminar flow reactor setup. Oxymethylene ethers with different number of oxymethylene ether groups (n=0-5) have been investigated under lean and rich conditions (750-1250 K). The flow reactor is coupled to an electron ionization molecular-beam mass spectrometer (EI-MBMS) with high mass resolution to measure speciation data. Additional isomer-selective speciation analysis was performed using a novel atmospheric laminar flow reactor combined with double-imaging photoelectron photoion coincidence (i2PEPICO) spectroscopy at the vacuum ultraviolet radiation (VUV) beamline of the Swiss Light Source. The results show a dominance of oxygenated intermediates during the combustion of all OMEs in the investigated temperature regime. The observed species pool is thereby nearly independent of the OME's chain length. In particular the presence of significant fractions of ethanol is remarkable and indicates unknown or underestimated reaction pathways to form C-C bonds from OME structures. Formation of combustion intermediates during oxidation of longer OMEs occurs at lower temperatures and correlates with the ignition delay time. No hydrocarbons with more than four carbon atoms are

detected. The combination of high mass resolution provided by EI-MBMS detection and isomer-selective analysis by i2PEPICO enables a complete overview of all intermediates. This allows for in-depth discussion and analysis of systematic trends for several intermediate species.

Keywords: Oxygenated fuels; Oxymethylene ethers (OMEs); Polyoxymethylene dimethyl ethers (POMDMEs); Photoionization molecular-beam mass spectrometry; i^{2}PEPICO

1. Introduction

Reducing the carbon footprint and greenhouse gas emissions have become a major driving force worldwide for fuels derived from renewable sources. In the wide range of applications, promising synthetic fuels as alternative or fuel additive in Diesel engines are oxymethylene ethers (OMEs). Diesel engines still play a major role in long distance transportation and 94 % of freight transportation with limited alternatives in short- to mid-term perspectives. OMEs, also commonly known as PODEs or POMDMEs (polyoxymethylene dimethyl ethers), have the general chemical structure CH_3-O-[-CH_2O-]$_n$-CH_3 with n as the number of CH_2O groups (see Fig. 1). They are oxygenated fuels and can be fundamentally produced in CO_2-neutral processes [1-3]. With no direct C-C bonds, oxymethylene ethers tend to form less soot during combustion processes [1, 2, 4]. Due to the low flashpoints of OME_1 and OME_2, as well as the high melting point of OME_6, an OME_{3-5} fuel mix is most suitable for use in current internal combustion engines [1, 5]. To investigate the decrease in soot as well as the increase in aldehyde emissions, a general understanding of the combustion chemistry of OMEs is required.

Several studies already addressed the combustion chemistry of OME_1 and OME_3. OME_1 was investigated in flow reactor environments by Marrodán et al. showing that the soot precursor acetylene (C_2H_2) is only occurring under pyrolysis conditions [6]. Vermeire et al. focused on the low-temperature oxidation of OME_1 in a jet-stirred reactor and developed a kinetic reaction model [7]. Jacobs et al. also generated a kinetic model for OME_1 oxidation at engine relevant conditions [8]. Focusing on premixed flat flames, Sun et al. investigated OME_1 and OME_3 with synchrotron vacuum ultraviolet (VUV) photoionization mass spectrometry [9-11] and developed a kinetic model for the combustion of these two OMEs. In their paper, they combined the investigation of laminar burning velocities of OME_3 flames and identification of different intermediates with synchrotron VUV photoionization mass spectrometry. He and coworkers provided another model for OME_3 and used ignition delay times measured by rapid compression machines alongside with theory for validation [12]. Ngugi et al. have studied laminar flame speed as well as ignition delay times and auto ignition of OME_{0-1} [13], as well as OME_2 [14]. They have shown that OME_2 reveals similar oxidation pathways compared to OME_1. This

is confirmed by the work of Eckart et al., where OME_1 and OME_2 reach their maximum burning velocity at the same equivalence ratio of 1.2 [15]. Cai et al. have recently demonstrated in shock tube experiments that the impact on fuel activity vanishes at high pressures with increasing length of the OME [16]. A rapid compression machine study of OME_2 and OME_3 show similar ignition delay times for high pressures, while for lower pressures the ignition delay times differ more [17]. Yu et al. investigated the unimolecular decomposition of OME_1 in a micro flow reactor. By applying PEPICO spectroscopy and quantum chemical computations they obtained a comprehensive potential energy surface. They suggested that the hydrogen migration and methanol formation to yield methoxymethylene carbenes (CH3-O-CH) are thermodynamically favored and direct C-H or R-O bond fission only plays a subordinate role, as previously suggested [18]. Kathrotia et al. have provided a new kinetic model including OME_{0-5} [19, 20], but speciation data for oxidation is absent in literature for the complete series of OME_{0-5}.

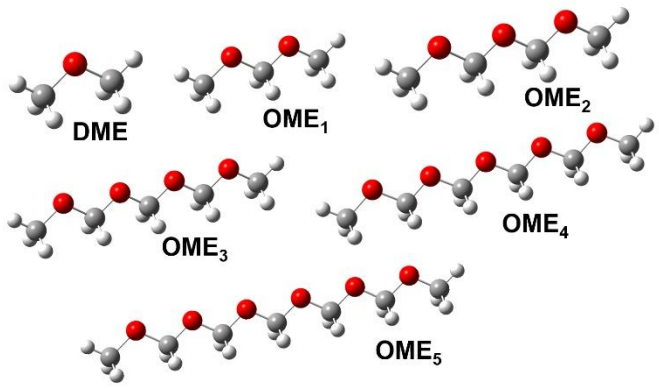

Fig. 1: Overview of all investigated OMEs

Here, a systematic investigation of the combustion chemistry of a series of oxymethylene ethers is presented to give a better understanding of the influence and effects of different chain lengths. Two complementary experimental setups are used to gain detailed information about the combustion process of OMEs. First, an atmospheric laminar flow reactor was used to investigate the combustion intermediate formation as a function of the reaction temperature. The series covers the full range of OME_n with n=0-5 i.e. it starts with dimethyl ether as the simplest OME and extend to OME_5. Special focus is on formation and mole fraction tendencies of combustion intermediates in relation to the chain

length of the fuel. Second, subsequent in-depth identification of oxidation intermediates with separation of isomers was performed at the i^{2}PEPICO endstation (X04DB) at the Swiss Light Source (SLS) using tunable synchrotron VUV photoionization mass spectrometry.

2. Experimental Setup

The study was performed using two experimental setups for a detailed systematic investigation of the series of oxymethylene ethers: the high-temperature atmospheric laminar flow reactor coupled to an electron ionization molecular-beam mass spectrometer (EI-MBMS) [12, 13] at DLR Stuttgart and the atmospheric laminar flow reactor setup coupled to the i^{2}PEPICO endstation [21-23] at the Swiss Light Source in Villigen, Switzerland. The DLR atmospheric flow reactor and the flame experiment at the i^{2}PEPICO endstation have been described elsewhere, so only a brief description is given here for both experiments. The new flow reactor setup at the i^{2}PEPICO endstation is developed on the basis of the DLR's reactor design and flow rates to ensure comparability. A smaller inner diameter has to be chosen so that the reactor fit into the experimental chamber of the i^{2}PEPICO endstation, but both reactors have similar flow velocities. The PEPICO reactor (PIRo) will be introduced and shown in greater detail here. The comparability of both reactor setups will be checked in section 3 based on their temperature profiles. For both experiments, DME (>99.9 % purity) was purchased from Linde and OME_1, also known as methylal or dimethoxymethane, from Sigma-Aldrich (>99 % purity). All larger OMEs were purchased from ASG Analytik and had a purity of ~98 %. Small amounts of OMEs with different chain lengths account for the remaining 2 %.

2.1 Atmospheric laminar flow reactor coupled to EI-MBMS at DLR Stuttgart

For each OME_n (n=0-5), a set of three different equivalence ratios (ϕ = 0.8, 1.2, 2.0) was investigated at DLR's atmospheric laminar flow reactor to get an overview from lean to very rich conditions. The experimental setup consists of an atmospheric high-temperature laminar flow reactor, which is coupled to an electron ionization molecular-beam mass spectrometry (EI-MBMS) system. The reactor is equipped with an alumina-ceramic (Al_2O_3) tube having an inner diameter of 40 mm and the reactor has an overall length of 1497 mm. Inlet conditions for all reactor measurements can be found in

Table 1. Flows of argon, oxygen, and fuels were controlled by Coriolis flow meters (Bronkhorst) to ensure a precise controlled flow rate. Liquid fuels were evaporated in a standard vaporizer system (Bronkhorst/CEM) with argon as carrier gas. Temperature of the vaporizer was set between 372.15 K for OME_1 and 473.15 K for OME_5. The vaporized fuel was fed over heating hoses to prevent condensation. Before entering the reactor, the fuel was premixed with oxygen and the remaining argon. Total argon dilution is about 99 % to avert heat release and self-sustaining reactions. The reactor has a reaction segment, i.e., a uniform temperature segment, with a total length of 1000 mm, 750 mm isothermal, heated by a customized high-temperature oven (GERO, Type HTRH 40-1000). The reactor diameter is chosen large enough to ensure the dominance of gas phase reactions. All measurements feature constant inlet flow conditions, while the oven temperature was linearly decreased (-200 K/h) from 1273–748 K. A relative precision of the measured reactor temperatures of ±5 K can be stated [24]. Residence times are depending on the chosen gas temperature and range from 2.8 s (750 K) to 1.7 s (1250 K).

For the MBMS system, gas is sampled at the end of the reactor by a quartz nozzle at the centerline of the reactor at ambient pressure (~960 hPa, 460 m above sea level). The nozzle has an opening of 50 µm. The molecular beam, which is formed by a two-stage expansion, is guided into an ion source of an electron impact (EI) time-of-flight mass spectrometer. The mass resolution of the spectrometer (R = 3000) is suitable to resolves the exact elemental composition (C/H/O) in this system. Ionization energy was set to 10.6 eV (actual peak value of electron distribution).

Table 1. Inlet flow conditions in standard cubic centimeter per minute (sccm at 273K; 1013 mbar) and initial mole fractions for high-temperature flow reactor measurements. Carbon flow was identical (corresponding to 50 sccm-C) for all conditions diluted by 9.9 slm argon.

	DME			OME1			OME2			OME3			OME4			OME5		
ϕ	0.8	1.2	2.0	0.8	1.2	2.0	0.8	1.2	2.0	0.8	1.2	2.0	0.8	1.2	2.0	0.8	1.2	2.0
Fuel / sccm	25.0	25.0	25.0	16.7	16.7	16.7	12.5	12.5	12.5	10.0	10.0	10.0	8.3	8.3	8.3	7.1	7.1	7.1
O_2 / sccm	93.8	62.5	37.5	83.3	55.6	44.4	78.1	74.4	44.6	75.0	50.0	30.0	72.9	48.6	29.2	71.4	47.6	28.6
x_{fuel} / 10^{-4}	25.0	25.0	25.0	16.7	16.7	16.7	12.5	12.5	12.5	10.0	10.0	10.0	8.4	8.4	8.4	7.2	7.2	7.2
x_{O2}/ 10^{-3}	9.4	6.3	3.8	8.3	5.6	3.3	7.8	5.2	2.8	7.5	5.0	3.0	7.3	4.9	2.9	7.2	4.8	2.9

2.2 Atmospheric laminar flow reactor coupled to the i²PEPICO spectrometer at the SLS

Figure 2 shows the design of the atmospheric flow reactor – PEPICO Reactor (PIRo). The design is based on the DLR atmospheric flow reactor. For utilization of an atmospheric laminar flow reactor at the i²PEPICO endstation, a reactor with a smaller diameter is needed due to available space fitting inside the experimental chamber. Its overall length is 1500 mm separated in a pre-heating zone of 500 mm with a constant temperature of 573 K and an adaptable heating zone of 1000 mm with an adjustable temperature range of 573-1123 K. Heating is provided by two heating sleeves by Horst GmbH. The reactor is equipped with a fused silica tube with an inner diameter of 22 mm and a thickness of 2 mm to prevent catalytic reactions during the oxidation of the fuel. The pre-heating zone provides controlled inlet conditions and prevents condensation of fuels with lower vapor pressures. For the adaption to the i²PEPICO system, the reactor is mounted in the experimental chamber of the i²PEPICO machine. The experimental chamber of the i²PEPICO machine remains open to provide the ambient pressure environment (970 hPa, 367 m above sea level). Gaining consistent flow conditions for the DLR as well as the i²PEPICO reactor, all flow rates used at the DLR reactor were scaled by the respective cross-sectional area, i.e. by a factor of 0.3 to ensure consistent resident times. Due to limited beamtime, a fuel-rich condition with the equivalence ratio of ϕ=1.2 was investigated. All flow conditions can be found in Table 2. Gas and fuel feeding were performed similar to the EI-MBMS system: Flows of argon, oxygen,

and fuels were controlled by Coriolis flow meters (Bronkhorst) to ensure a precise controlled flow rate. Liquid fuels were evaporated in a standard vaporizer system (Bronkhorst/CEM) with argon as carrier gas. Temperature of the vaporizer was set between 372.15 K for OME_1 and 473.15 K for OME_5. The vaporized fuel was fed over heating hoses to prevent condensation. The argon dilution was set to 99%. In contrast to the measurements at DLR's reactor, all temperatures were set individually and measurements were started, when thermal equilibrium was reached. Residence times are similar to the DLR reactor by design, ranging from 2.8 s (750 K) to 2.1 s (1006 K). At the chosen gas temperatures for the energy scans, residence times are 2.2 s (959 K) for OME_1 and 2.4 s (866 K) for $OME_{3\text{-}5}$.

To ensure sampling from atmospheric pressure, a quartz nozzle with an orifice of approximately 33 µm was used. Residuals gases were pumped out of the i^{2}PEPICO experimental chamber immediately. Rapid expansion of the sampled gas into high vacuum forms a molecular beam, which is guided through a skimmer into the ionization chamber. Synchrotron VUV radiation within the range of 6–21 eV, provides soft photoionization (see Fig. 2). The i^{2}PEPICO spectrometer [25, 26] enables simultaneous detection of electrons and ions formed during the same ionization event in a photoelectron photoion coincidence scheme (PEPICO). Both, photoelectrons and photoions are two-dimensionally imaged on micro channel plate (MCP) detectors with delay anodes (Roentdek, DLD 40) [26]. Used as a trigger signal in a multi-start/multiple-stop coincidence scheme, electrons are used to start the time-of-flight mass spectrum, so each electron can be assigned to a single ionization event, enabling the measurement of mass-selected threshold photoelectron spectra (ms-TPES). Therefore, threshold electrons close to the center of the detector (see Fig 2.) and so-called "hot-electrons", with significant kinetic energy but negligible off-center momentum, are subtracted following the data evaluation by Sztáray et al [26, 27]. These ms-TPES are following the Franck-Condon principle. Having the photoions also mapped at the i^{2}PEPICO setup, the molecular beam can clearly be distinct from the background, due to its higher velocity (see Fig. 2).

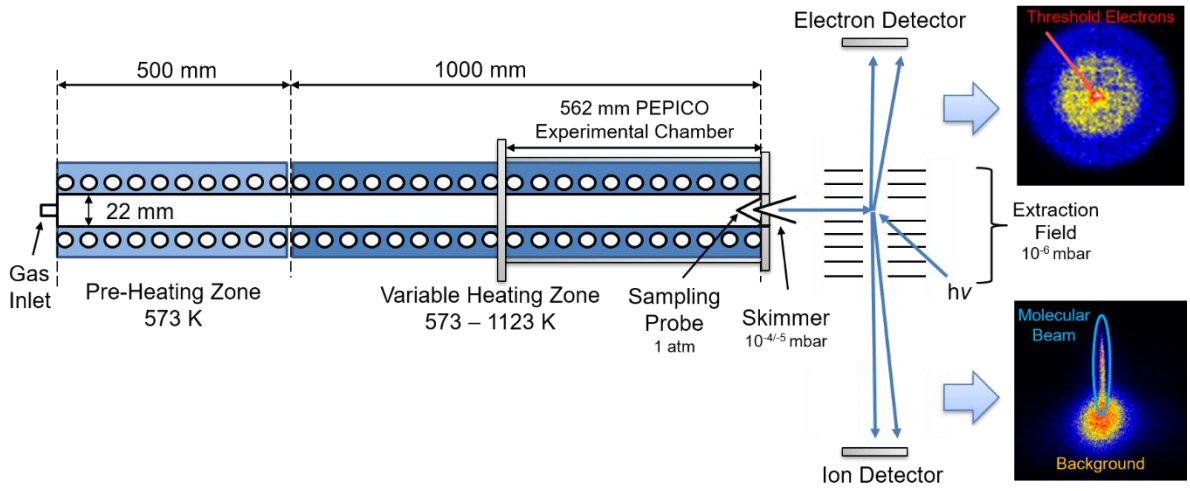

178

179 **Fig. 2:** Schematic sketch of the double-imaging photoelectron photoion coincidence (i^{2}PEPICO) setup
180 for atmospheric flow reactor sampling molecular beam mass spectrometry (MBMS). PEPICO reactor
181 (PIRo) design and setup is displayed.

182 **Table 2: Flow conditions for atmospheric laminar flow reactor measurements at the i²PEPICO**
183 **endstation with a constant carbon flow of 15 sccm. Equivalence ratio is set on ϕ=1.2 for all**
184 **conditions. All temperatures given are gas temperatures.**

	Ar/slm	Fuel/sccm	O_2/sccm	x_{fuel} /10^{-4}	x_{O2} /10^{-3}	Temperature/K Ramp	Temperature/K Energy Scans
OME_1	2.97	5.0	16.7	16.7	5.6	723 – 1006	959
OME_3	2.97	3.0	15.0	10.0	5.0	723 – 959	866
OME_4	2.97	2.5	14.6	8.4	4.9	723 – 959	866
OME_5	2.97	2.2	14.3	7.3	4.8	723 – 959	866

185

186 **2.3 Data evaluation and uncertainties**

187 Data evaluation follows the established procedures described in [24, 28] for EI-MBMS and [21, 23, 29]
188 for i^{2}PEPICO experiments. The short overview as follows: For EI-MBMS experiments, the integrated
189 and corrected ion signals are connected to their mole fractions (x_i) by comparison to the respective signal
190 of the non-reactive species argon. Correction for background and fragmentation of species through the
191 ionization process are performed with consideration of fragmentation patterns of the calibrated species.

Due to soft ionization at the i²PEPICO reactor experiment, no fragmentation correction except for the fuel was necessary for the measured species. If needed, signals were corrected for contributions of ^{13}C isotopes. For both experiments, mole fractions of major species are calculated from direct calibration with CO/CO_2 mixtures and internal calibration by element balances of C, H, and O. Labile species were not directly calibrated, but quantified by the relative ionization cross section (RICS) method [30] for the electron ionization experiment. In the i²PEPICO experiment, typically photoionization cross sections from the literature are used for quantification. For the EI-MBMS signal in the DLR reactor setup, the statistical and relative uncertainty is below 10 % [28]. For species using direct calibration, uncertainty ranges between 15–20 %, while for non-calibrated species the uncertainty can increases to a factor of 2–4. For the i²PEPICO reactor setup, the uncertainty is estimated to be between 30–50 % for intermediate species with measured photoionization cross sections regarding the error from literature [22, 31]. For species with unknown cross sections, the uncertainty increases up to the factor 2–4.

3. Results and Discussion

The systematic investigation of oxidation of OMEs with different chain lengths (n=0-5) is presented here. To validate different OME intermediates, $OME_{1,3,4,5}$ were investigated at the i²PEPICO spectrometer with a focus on intermediate detection and isomer separation. For the first time, a complete overview of the oxidation of a full series of OMEs was conducted.

To support the interpretation of some results gained in this study, the DLR reaction mechanism by Kathrotia et al. [20] was used to provide rate-of-production analysis for ethanol at the 866 K (the temperature of the PIE scan) as well as comparison of experimental results with models by Jacobs [8], Sun [11], and Kathrotia [20] using the plug flow reactor module with a predefined temperature profile within the Chemical Workbench [32]. Temperature profiles can be found in Fig. 3 and Fig. 4 as well as in the supplementary material.

3.1 Temperature profiles

To ensure comparability of both experimental setups, gas temperatures are used when comparing both reactors in contrast to most previous flow reactor studies, in which the preset oven temperature was used

as the corresponding x-axis temperatures [19, 24, 28]. A slight systematic deviation to the actual gas temperature is known but was typically only corrected for comparisons to model calculations. Since the correct temperature profile of the PEPICO reactor is mandatory for comparison with the DLR reactor as well as for proper kinetic interpretation, temperature profiles for the applied flow conditions were taken. For the PEPICO reactor, temperature profiles were measured along the longitudinal axis of the flow tube. A type N thermocouple with a length of 1600 mm and a thickness of 0.5 mm by OMEGA was used. The thermocouple was neither isolated nor coated and provides a temperature uncertainty of less than 4 K by its specifications. The thermocouple itself was encased by a silica tube with a thickness of 6 mm, which can be placed at any position on the reactor centerline. Temperature profiles are measured by successive downstream translation of the thermocouple for specific reactor temperatures and a constant argon flow of 2.97 slm. The pre-heating zone is set to 573.15 K, while the main heating zone is set to different temperatures between 573.15 – 1173.15 K. The spatial distance is measured in respect to the reactor inlet. To ensure correct temperature measurements, recording starts when thermal equilibrium is reached. The gas temperature according to the set reactor temperature can be seen in Fig. 3: only a small isothermal zone between 1100-1350 mm was formed. The difference between the set reactor temperature and the measured gas temperature are a direct result of the narrowed thermal isolation of the heating sleeves. No scaling law can be adapted to determine the gas temperature due to the unsteady isothermal zone. Therefore, all valid reactor temperatures were set and directly measured maximum gas temperature for each specific reactor temperature is used. In the following, the maximum measured gas temperature is referred to as “gas temperature”. Comparison of different main and intermediate species’ profiles have proven the comparability of both reactors using the respective gas temperatures and will be shown later.

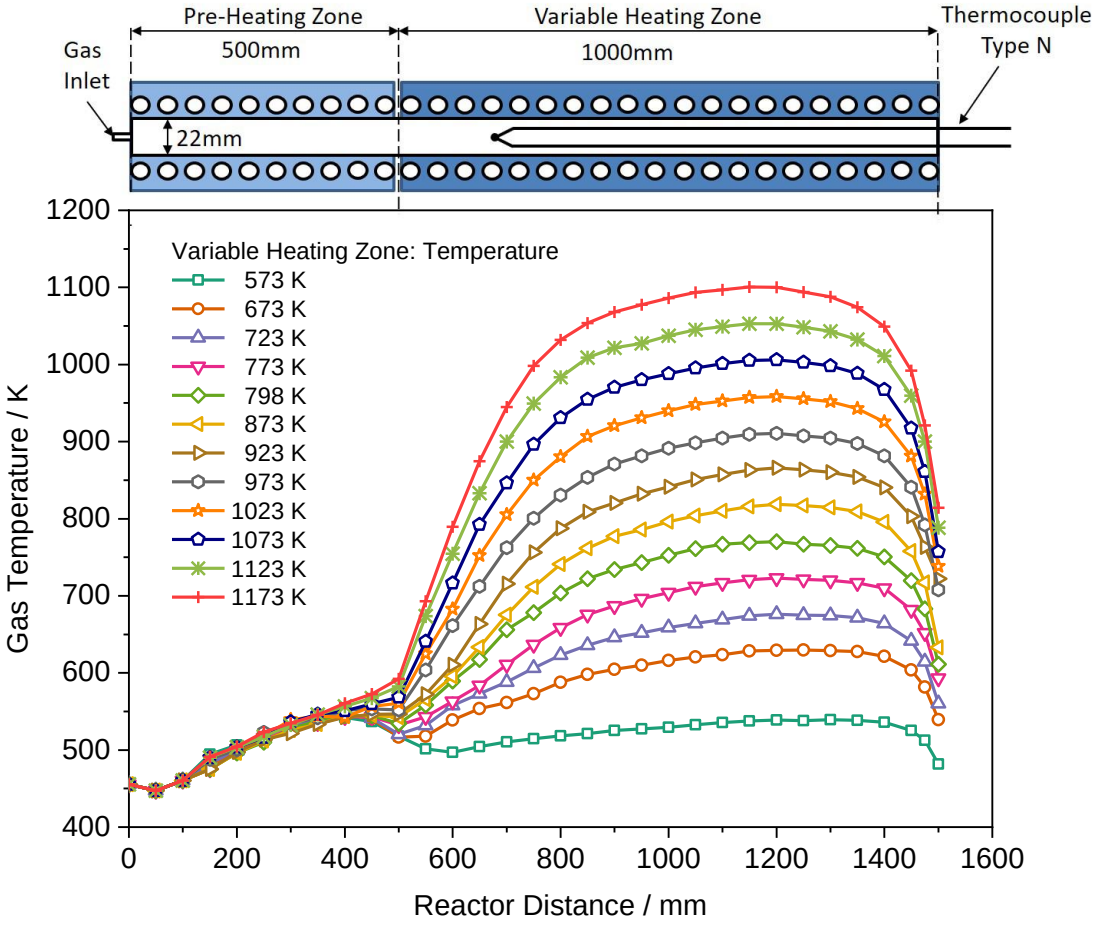

240

241 **Fig. 3**: Measured temperature profile for PEPICO reactor (PIRo).

242 Temperature profiles for the DLR flow reactor are already published by Oßwald et al. [28] and can be
243 seen in Fig. 4. It was shown that an isothermal region between 600 – 1300 mm is formed by the applied
244 flow conditions of 10 slm. To ensure comparability between both used reactors, re-measurements of the
245 temperature profile were obtained using the same thermocouple used for the PEPCIO reactor. A fixed
246 position in the isothermal region was chosen for the measurements. Temperatures were recorded when
247 thermal equilibrium has been reached. Correction of radiative heat loss has not been applied due to the
248 negligible temperature difference to the reactor wall. The temperature data set measured by Oßwald et
249 al. [24] could be confirmed and the equation was updated [28] to the following:

250 $$T_{Gas\ flow}(x)\ [K] = (T_{ref}(x) - T_0) \cdot \frac{(0.9931 \cdot T_{Oven} + 15.46\ K) - T_0}{T_{ref}(1000\ mm) - T_0} + T_0 \quad [1]$$

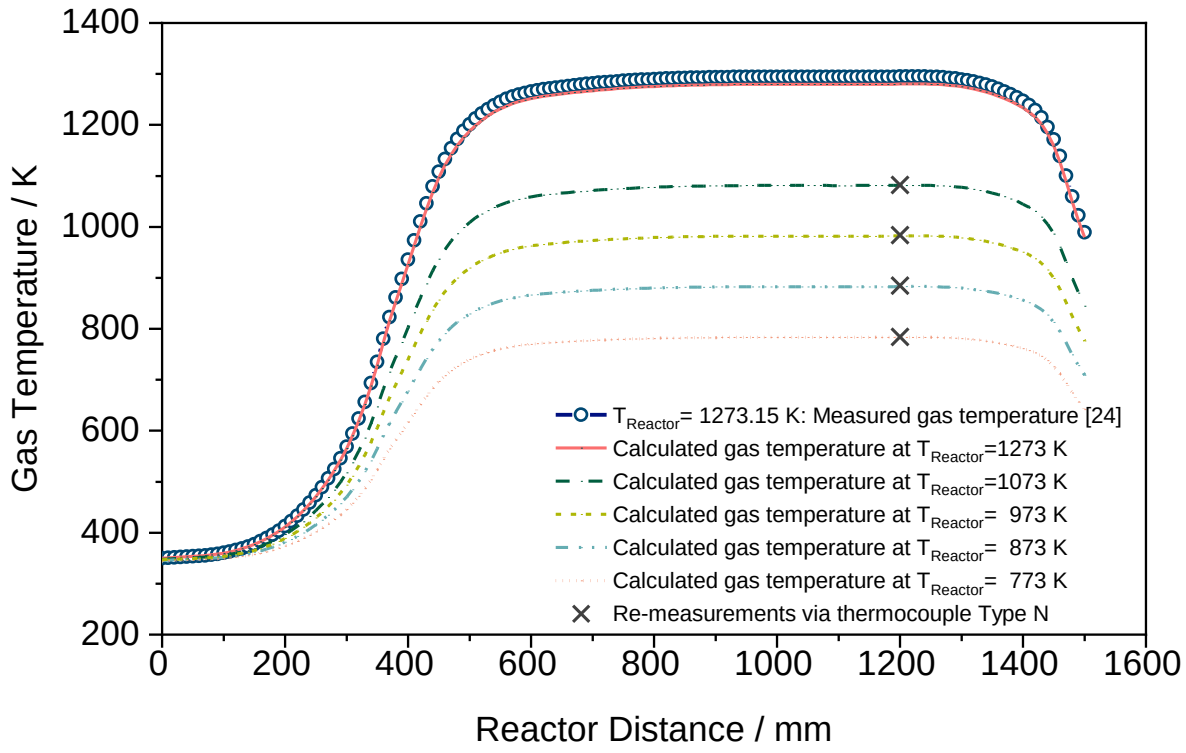

Fig. 4: Centerline temperature profiles for a constant oven temperature of 1273.15 K [24]. Lines are representing the T_{ref} = 1273.15 K scaled by the respective oven temperature ratio. Re-measurements of gas temperatures for specific $T_{Reactor}$ via thermocouple type N are displayed.

3.2 Comparison of the complementary reactors

Mass spectrometric investigation of the OME oxidation reaction is complicated by the fact that similar to OME_1, all higher OMEs do not form stable molecular ions through electron ionization and photoionization [11, 33] and instantaneously fragments towards smaller ions. A fragment is used for the evaluation of the fuel signal in EI-MBMS: C_2H_6O is chosen for DME, $C_3H_7O_2$ for OME_1 and $C_4H_9O_3$ for all higher OMEs. Even though soft ionization is provided through the synchrotron VUV light source, all OME measurements are also complicated by the absence of a stable parent ion and show a variety of fragments. However, fuel fragmentation was corrected properly, but prohibits a direct measurement of the fuel radicals [23].

The i^{2}PEPICO experiment allows isomer-selective species identification using i^{2}PEPICO spectroscopy but due to the low mass resolution isobaric species must be considered. The i^{2}PEPICO results are focusing on characteristic mass-to-charge ratios (m/z) and identifies several intermediates on the basis

of their photoionization efficiency curves (PIE) as well as their threshold photoelectron spectra (TPES). Quantification and overall comparison between different stoichiometric conditions are gained via EI-MBMS results, which concludes the systematic investigation on the DLR atmospheric reactor. The results gained here give a broad quantitative overview on the chemical species involved and are provided for model validation purposes with this contribution, while we are going deeper into the combustion chemistry and add another layer by adding identifications of relevant isomers by the i^{2}PEPICO setup. Furthermore, the analysis of the photoionization data is used to validate calibration factors applied on EI-MBMS data.

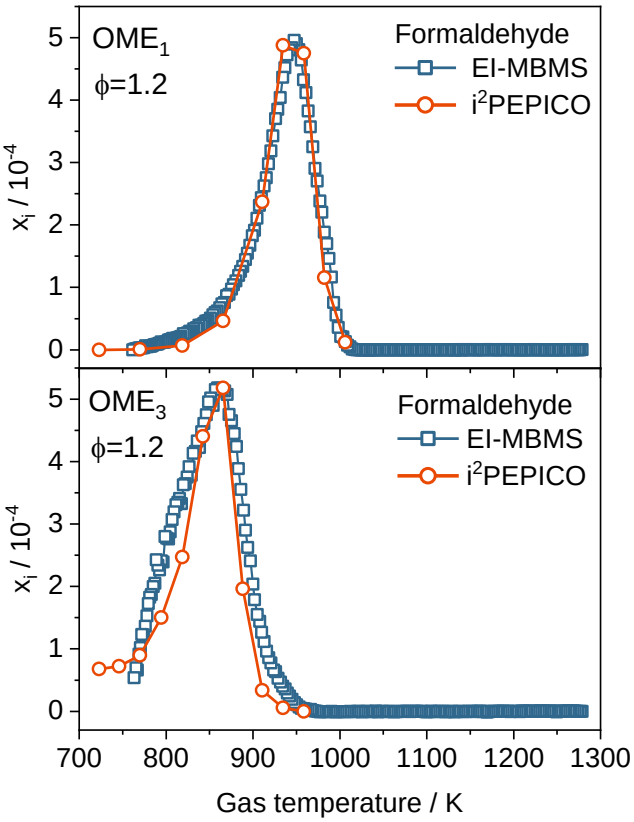

Fig. 5: Comparison of mole fraction profiles of formaldehyde measured for OME_1 and OME_3 by EI-MBMS and i^{2}PEPICO for equivalence ratio of ϕ=1.2. Temperatures are given in gas temperatures.

279 Figure 5 shows the mole fraction profiles of formaldehyde measured by EI-MBMS and i^{2}PEPICO on
280 the example of OME_1 and OME_3. For EI-MBMS, gas temperatures are calculated by using equation 1,
281 while for i^{2}PEPICO, gas temperatures were directly measured at the isothermal region (Fig. 3). As it can
282 be seen here on the example of formaldehyde in OME_1 and OME_3, a clear fit of both detection methods
283 can be observed using gas temperatures. Therefore, the results of both used reactors and detection
284 methods are valid and comparable. The fact that both reactors supply similar results, even though they
285 have significant difference in diameter and volume/surface ratio, supports the initial assumption that
286 surface reactions are negligible in these setups. Choosing the temperature for the energy scans, the
287 maximum of the formaldehyde peak was used. Note that this chosen temperature is not the optimum
288 condition for the separation of all intermediates, but was the best compromise to gain strong signals for
289 all intermediates at a single energy scan with long averaging times and a ΔE=0.025 eV. Due to the high
290 dilution of the gas mixture and the limited beamtime, we can only provide profiles of intermediates,
291 having a strong mole fraction and signal intensity.

292

3.3 Main oxygenated intermediates

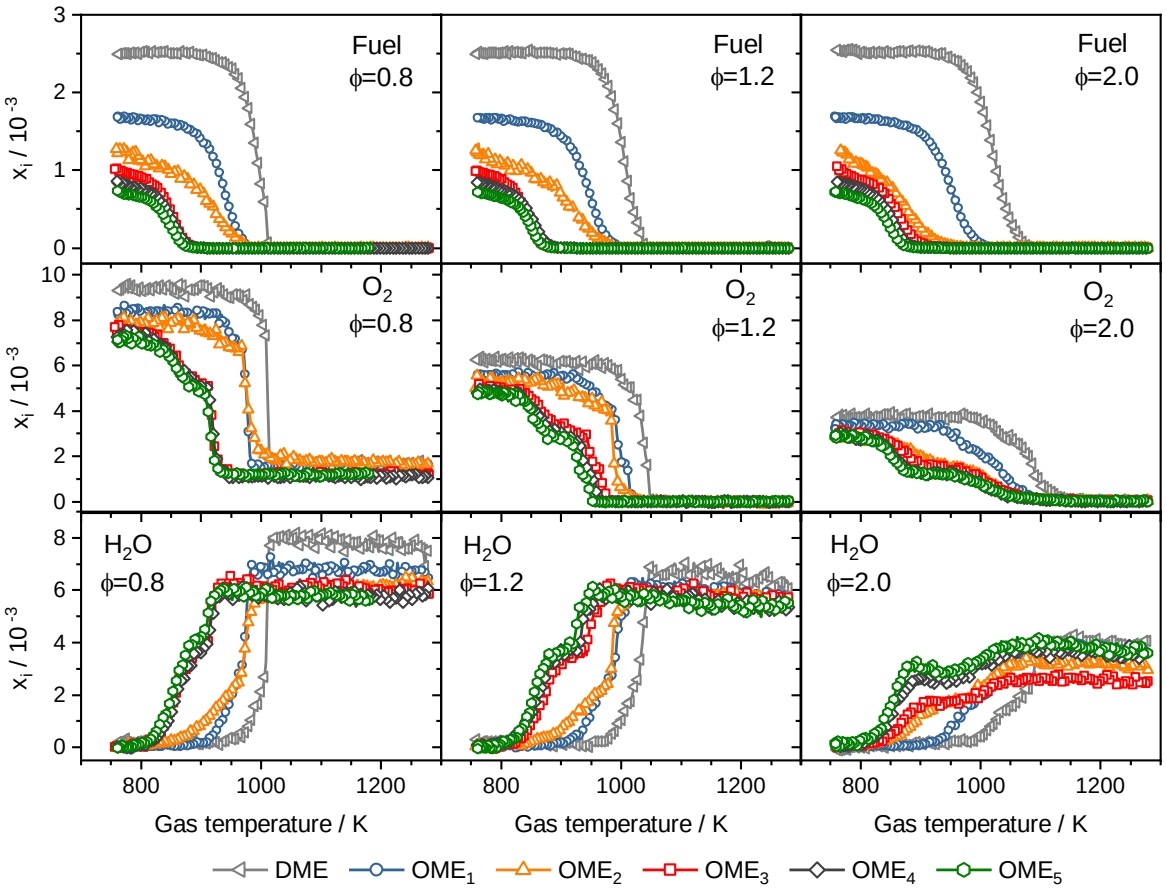

Fig. 6: Mole fraction profiles of fuel, oxygen (O_2) and water (H_2O) for oxidation of OMEs at different equivalence ratios. Number of plotted datapoints is reduced for clarity. Uncertainty is ± 20 % for all species.

Figure 6 shows mole fraction profiles of the used fuel, oxygen and water, as an example of the main species. In general, long-chain OMEs (OME_{3-5}) are completely consumed at lower temperatures compared to $OME_{0-2,}$ hence a lower number of oxymethylene ether groups correlates with higher reaction temperatures, i.e., lower reactivity. This observation directly corresponds to the ignition delay time [5, 16, 34, 35]. It is also notable that OME_2 is tending to react more like DME and OME_1 for stochiometric conditions of 0.8 and 1.2, while for very fuel rich conditions (ϕ=2.0), the reaction behaviour is similar to OME_{3-5}.

Furthermore, a pronounced step can be seen in the main species profiles of OME_{3-5} as well as OME_2 (ϕ=2). Such a step in the main species' profiles was already observed in other oxidation studies, as for example for the oxidation of ethanol [36]. Detecting such a step in the species profiles indicates that the residence time of the gas mixture in the reactor is long enough to observe the onset of an NTC-region (negative temperature coefficient) or rather the ignition delay time of the chosen condition is fast enough to observe NTC-behavior. Note that significant larger residence times at typically needed to observe the full low temperature chemistry in these reactor setups [28]. The ignition delay time is thereby very sensitive to the stoichiometry [37]. Niu et al. have recently published a paper investigating the ignition delay times for OME_{1-6} under different pressures and stoichiometry [35]. They have shown that the discrepancy in ignition delay times between two adjacent OME_n is getting smaller with the length of the OME. This correlates with the cetane number of the OMEs [5, 16, 34]. This is why a step can be seen in the mole profiles for OME_{3-5}, but not for OME_{0-1} where the residence time is too short for NTC. Regarding the different behaviour of OME_2 for lean and fuel rich conditions, Niu et al. could show that for ϕ=0.5 the ignition delay time is slower than for ϕ=1.0 than for ϕ=2.0: the ignition delay time gets faster with the stoichiometry. Therefore, we conclude that for OME_2, the chosen conditions (p=1 atm, residence times: 2.8 s - 1.7 s) are directly in between the ignition delay times, where the behaviour shifts from detecting the NTC region (ignition delay is short enough for chosen residence time) for ϕ=2, and being too fast at ϕ=0.8 and ϕ=1.2.

In Fig. 7, mole fraction profiles of most abundant intermediates are shown. All of them are oxygenated species. Since most detected signals have been seen constituted by different isomers, the calibration was chosen according to the main isomer: CH_2O is calibrated as formaldehyde, CH_3OH as methanol, and C_2H_6O as a combination of ethanol and dimethyl ether, which will be specified in section 3.4. CH_2O_2 is quantified as formic acid, whereby RICS was applied using ethanol as reference [30]. $C_2H_4O_2$ is calibrated as methyl formate that was also identified by Peukert et al. as stable reaction product during thermal decomposition of OME_1 [2].

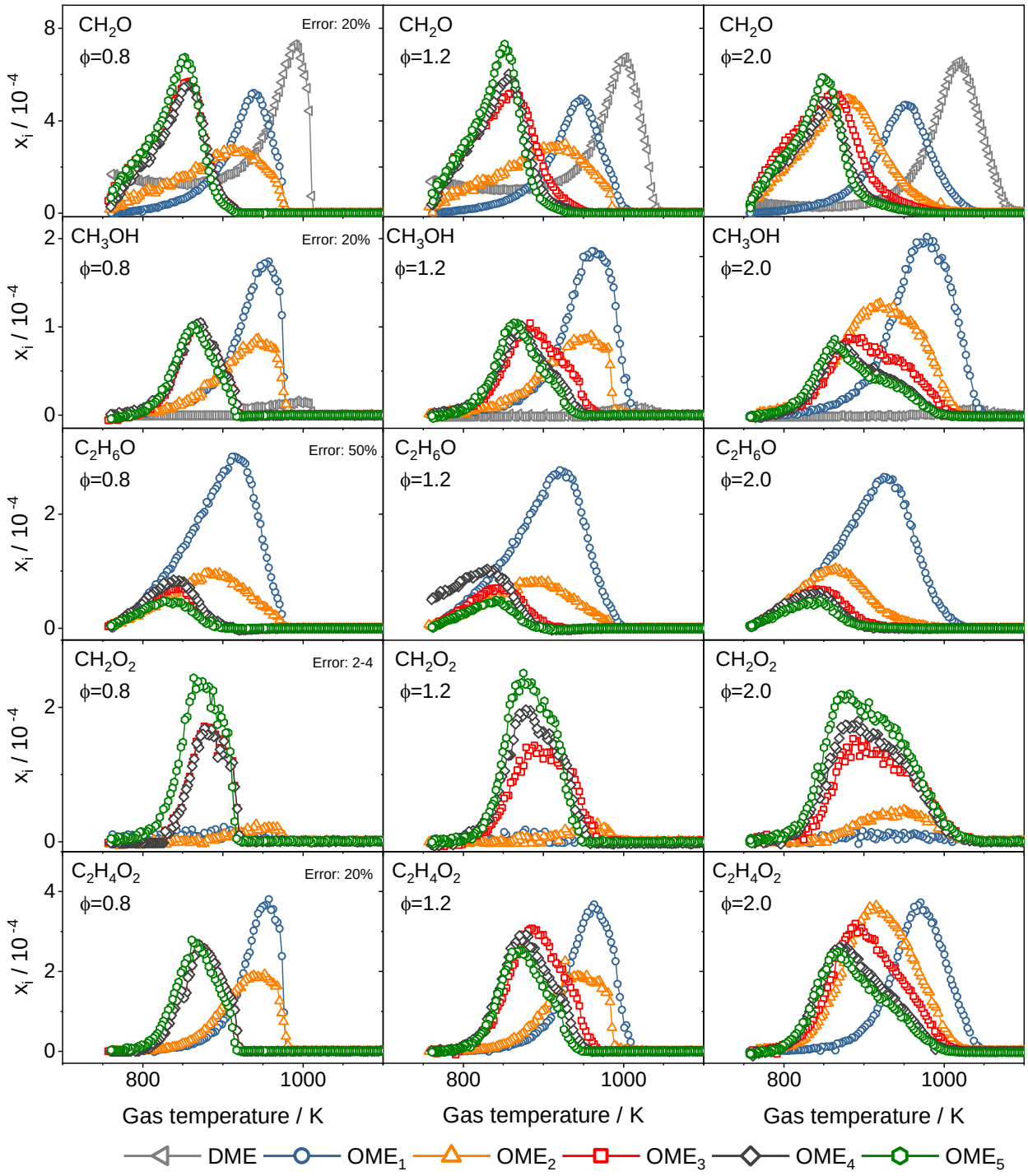

330

331 **Fig. 7:** Mole fraction profiles of formaldehyde (CH_2O), methanol (CH_3OH), dimethyl ether/ethanol
332 (C_2H_6O), formic acid (CH_2O_2), and methyl formate ($C_2H_4O_2$) for oxidation of OMEs at different
333 equivalence ratios. Uncertainty for each species is displayed in the first column.

334 For all OMEs, oxygenated species are the dominating intermediates with formaldehyde as the one with
335 highest mole fraction. In all investigated fuels and stoichiometries, methanol and methyl formate peak

at the same temperatures and in similar concentrations. This can be interpreted as confirmation of the methanol formation process stated by Peukert et al. [2]. They showed that one main formation way for methanol is from methyl formate during thermal decomposition of OME_1. Methyl formate is thereby built via two reactions initiated either by a) bond cleavage or by b) H-abstraction. According to [2], the H-abstraction is favored.

a) $CH_3OCH_2OCH_3 = CH_3 + CH_3OCH_2O$

$CH_3OCH_2O = H + CH_3OCHO$

$CH_3OCHO = CO + CH_3OH$

b) $H + CH_3OCH_2OCH_3 = H_2 + CH_3OCHOCH_3$

$CH_3OCHOCH_3 = CH_3 + CH_3OCHO$

$CH_3OCHO = CO + CH_2OH$

Indeed, for $OME_{1,3-5}$, methyl formate is also directly identified by its threshold electron spectra, as it can be seen on the example of OME_1 and OME_5 in Fig. 8. Other isobaric species at m/z=60 as methoxy ethane or propanol (C_3H_8O) are not detected in both reactor setups. $C_2H_4O_2$ calibrated as methyl formate in the EI-MBMS setup is therefore validated. A similar behavior can be seen for OMEs with longer chain length: less methyl formate and consequently less methanol is produced, but both intermediates appear at the same temperatures for all OMEs. This hints to the fact that methanol is produced through dissociation of methyl formate for all chain lengths. Another formation channel for methanol in thermal decomposition of OME_1 was found by Yu et al. [18]: They suggest that the hydrogen migration and methanol formation to yield methoxymethylene carbenes (CH_3-O-CH) are thermodynamically favored and direct C-H and R-O bond only plays subordinate role as previously suggested. Due to the similar decomposition behaviour of all OMEs, it can be assumed that this methanol formation route is also applicable for all higher OMEs. Ren et al. proposed in their shock tube study further decomposition pathways of methyl formate: $CH_3OCHO = CO_2 + CH_4$ and $CH_3OCHO = HCO + CH_3O$ [38-40]. For DME oxidation, no methyl formate and therefore only a small amount of methanol is formed. Also, the formation way by Yu et al. is not adaptable for DME. At the current state, no final conclusion about the

main pathways can be drawn, noticeable effort in the model development have to be drawn. Main focus here is the discussion and sharing of the experimental findings.

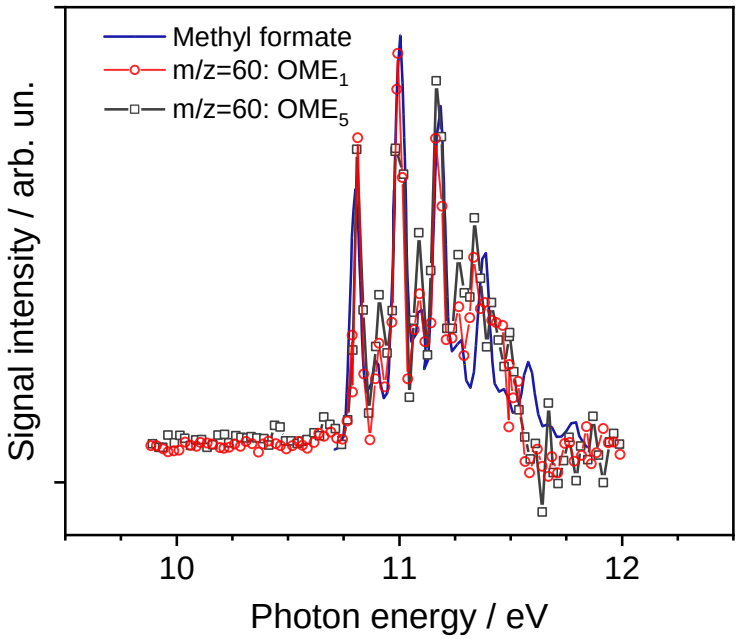

Fig. 8: Threshold photoelectron spectra (TPES) of *m/z*=60 in comparison with literature spectra [41-43].

For all OMEs, the intermediate species pool is very similar. Small oxygenated species discussed in the oxidation of OME_1 are therefore also relevant during the oxidation for higher OMEs. The largest detected species are methyl formate for all fuels and OME_1 in the OME_{2-5} fueled measurements. Accordingly, higher OMEs must undergo a rapid decomposition into smaller fragments. All OMEs are "burning from the end": main decomposition pathways are thereby primarily initiated by forming the primary radicals i.e. by H-abstraction from the terminal CH_3 moiety of the initial OME_n, which is afterwards directly decomposed to next smaller primary OME_{n-1} radical and formaldeyhde, and so on. This is also underlined by the fact that the same intermediates, i.e., CH_2O, C_2H_4O, and $C_2H_4O_2$, appear at similar temperatures for the fuels OME_{3-5}. Sun et al. have shown with their simulations for OME_{1-3} that a longer chain length of OMEs leads to an enhanced carbon flux to CH_2O and less to CH_3 [10]. The concentration raise of formaldehyde for larger OMEs cannot be seen at the conditions investigated herein. Especially the higher OME_3, OME_4 and OME_5 show very similar concentrations for

formaldehyde, while for OME_2 a smaller mole fraction of formaldehyde is observed compared to all other OMEs. Note that low-temperature chemistry was not investigated in this presented study [44]. Except for DME oxidation, reactivity can already be seen at low temperature, leading to substantial formation of formaldehyde even below 770 K. OME_{3-5} show the onset of a low temperature regime in all investigated conditions, as it can be seen in Fig. 6 from small steps in the profiles of oxygen and water. It should be noted that in particular OME_2 clearly shows this onset for the rich conditions (ϕ = 2.0) but less for the leaner condition (ϕ = 1.2 and 0.8). As a consequence, OME_2 profiles are found to be closer to the shorter OMEs for the lean conditions and closer to the longer OMEs at the ϕ = 2.0 measurement.

3.4 Formation and impact of C-C bonds

No soot precursors like benzene, typically observed during oxidation of hydrocarbons and other oxygenated fuels (e.g., higher alcohols) [45, 46], can be detected under the investigated conditions. This holds for even very fuel-rich conditions (ϕ =2.0). Figure 9 shows ethylene (C_2H_4) and propene (C_3H_6) profiles for all fuels. Beyond these intermediates, the longest detectable carbon chain in the complete series are butadiene (C_4H_6) and 1-butene (C_4H_8) using EI-MBMS, with a maximum mole fraction of $1.4 \cdot 10^{-7}$. Note that this is very close to the detection limit of the EI-MBMS system and even possible due to the high ionization cross section of these species. Therefore, no trend between the different chain lengths of the OMEs can be derived. For carbon chain lengths of C_2 and C_3, a trend can be seen as on the example of ethylene and propene (Fig. 9): higher OMEs tend to form less species with C-C bonds. The main reaction pathway for the formation of hydrocarbons is over methyl radical recombination reaction ($CH_3 + CH_3 = C_2H_6$). In general, available models for OME combustion [8, 11, 12, 20] show good prediction of hydrocarbon formation (Fig. 13). For higher OMEs, models can still be optimized. Data for all other hydrocarbons, e.g. CH_3, C_2H_2, C_4H_6 and C_4H_8, can be found in Supplementary 1 as well as the maximum mole fraction in Supplementary 2.

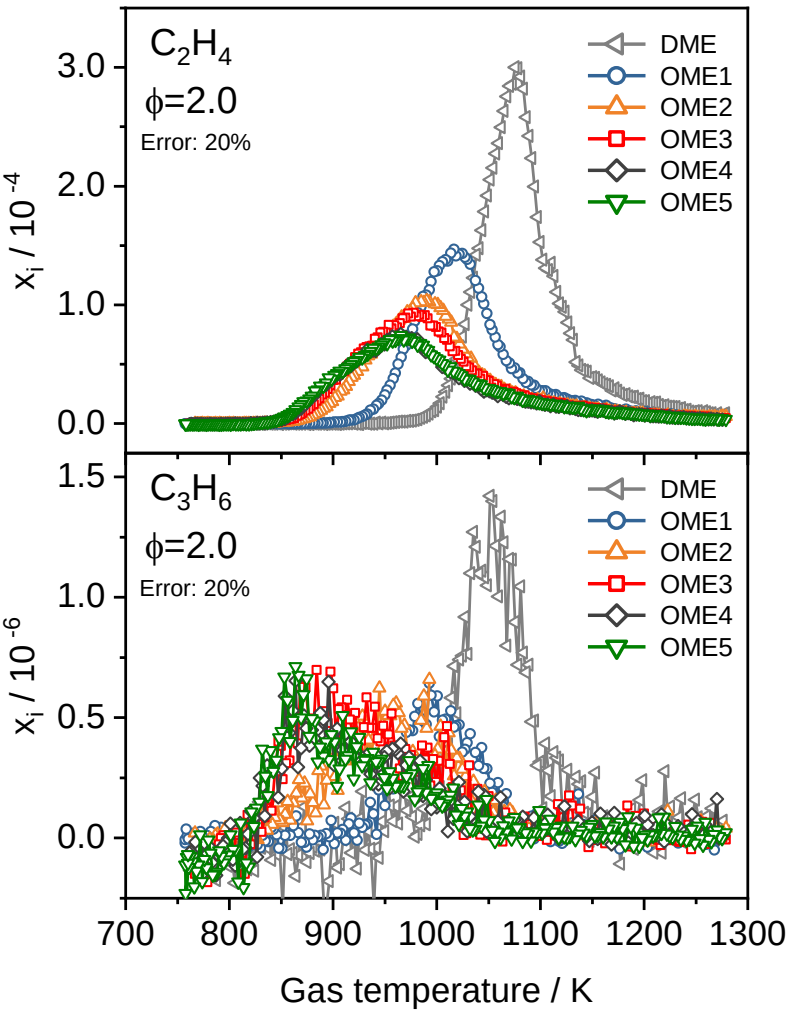

403

404 **Fig. 9:** Mole fraction profiles of ethylene (C_2H_4) and propene (C_3H_6) for oxidation of OMEs at

405 equivalence ratio of ϕ=2.0. Uncertainty for each species is displayed.

406

Identification of m/z=46

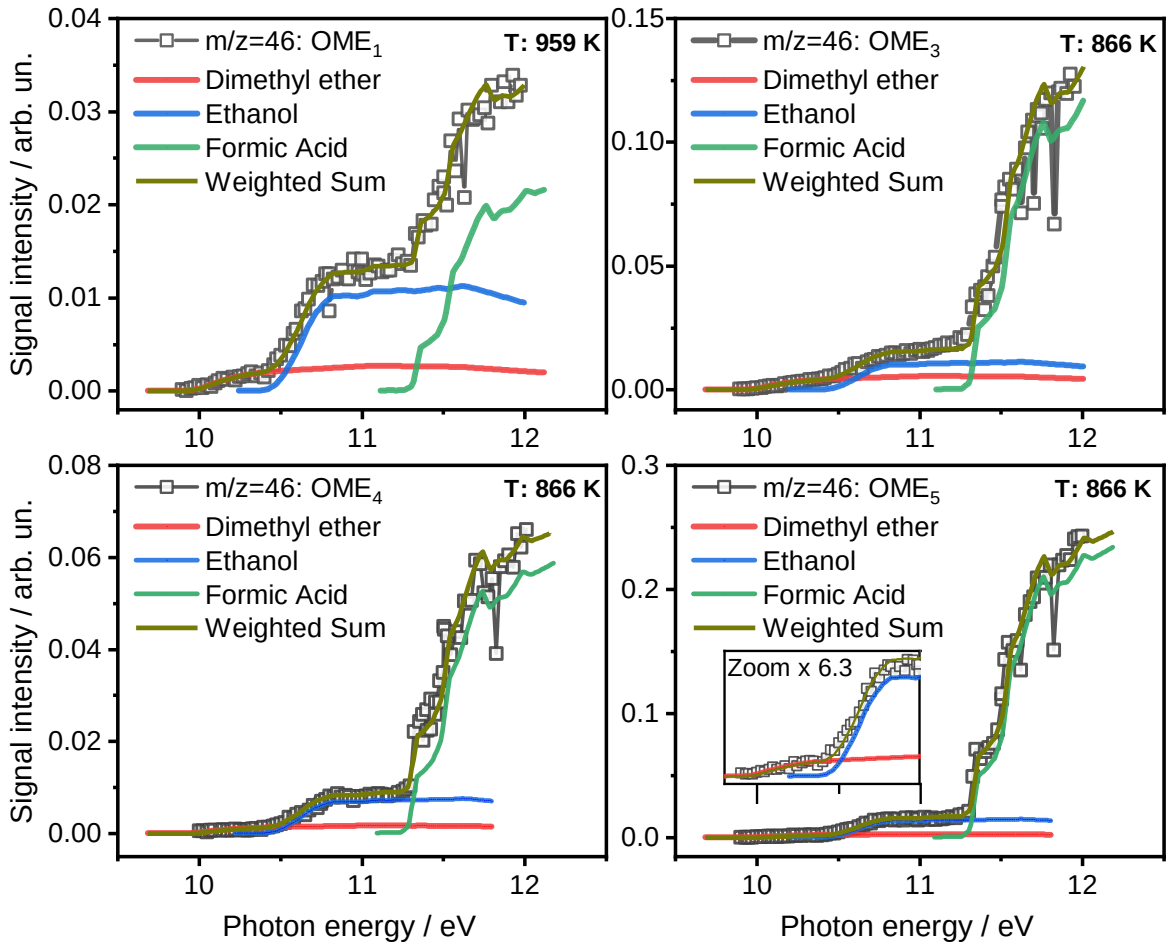

Fig. 10: $OME_{1,3-5}$ photoionization efficiency curves (PIE) of *m/z*=46 at a gas temperature of 959 K for OME_1 and 866 K for OME_{3-5} in comparison with PIE literature spectra of dimethyl ethyl, ethanol and formic acid, and their weighted sum [47, 48].

Low concentrations for long chain hydrocarbon intermediates, however, are not unexpected for a highly oxygenated fuel such as the OME fuels. Oxygenated intermediates on the contrary show a significant contribution to species exhibiting a carbon-carbon bond. Figure 10 for example shows the photoionization efficiency curves (PIE) of *m/z*=46 for $OME_{1,3-5}$ and compares the measured PIE curves to the weighted sum of respective literature photoionization cross sections. Weighting factors i.e. mole fraction ratios, are summarized in as shown in Table 3. The match proves the presence of dimethyl ether,

formic acid and ethanol in all investigated conditions and ethanol was found to be the dominating isomer.

The low signal-to-noise ratios do not allow to provide threshold photoelectron spectra for m/z=46- Furthermore, due to the too low signal intensities at the temperature scans, ethanol and dimethyl ether cannot be separated for the complete temperature range for $OME_{1,3,4}$. Only for OME_5, an intermediate profile of dimethyl ether was obtained via photoionization and quantified via direct calibration of DME. The separated mole fraction of dimethyl ether and ethanol can be seen in Fig 11. Photoionization energy of 10.3 eV is used for the pure DME signal, while ethanol is calculated by the summed signal measured by EI-MBMS subtracted by DME, using literature photoionization cross section [32]. Overall quantification is done by the EI-MBMS signal.

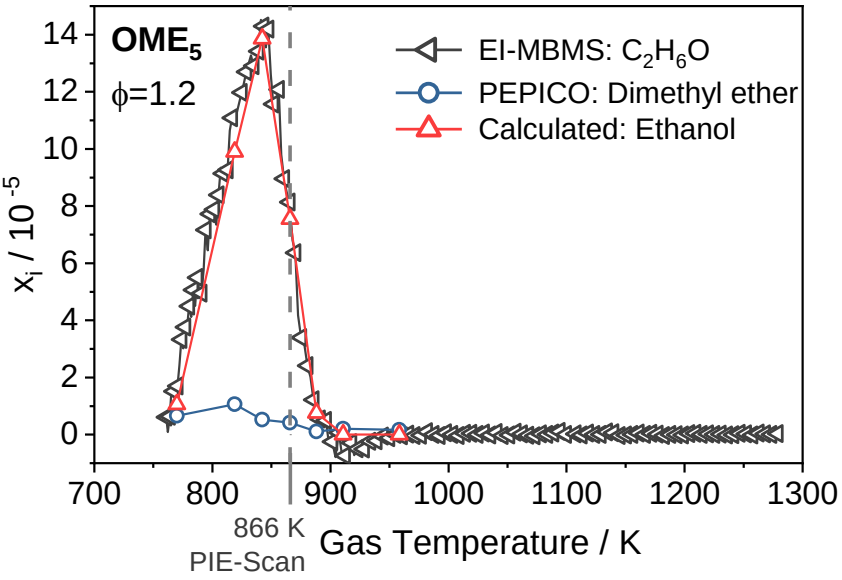

Fig. 11: Mole fraction of dimethyl ether and ethanol separated by photoionization energy of 10.3 eV. The respective temperature of the PIE scan is indicated. For combined C_2H_6O mole fraction measured by EI-MBMS, every second measured point is displayed.

Formic acid can also be confirmed for OME_1 in the PEPICO results, while no formic acid could be detected in the EI-MBMS setups. This can be traced back to the higher detection sensitivity of the i^2PEPICO experiment. Note that the chosen gas temperatures are ~23-39 K higher than the maximum peak temperature of C_2H_6O for each OME, but the mole fraction at these temperatures are still high

enough to separate DME and ethanol. Quantitative fractions of dimethyl ether and ethanol are provided in Table 3. For all measured OMEs, the mole fraction of ethanol is higher than for dimethyl ether for the chosen gas temperatures. The obtained isomer ratio was considered for quantification of the EI-MBMS signal by applying weighted calibration factors for the actual C_2H_6O isomer mixture. For the equivalence ratios of 0.8 and 2.0, for each OME, the same calibration factor as for 1.2 was assumed. Note that this is a first approximation since the isomer ratio seen in the PEPICO experiment may change with temperature and stoichiometries. Photoionization curves of ϕ = 0.8 and 2.0 series have not been measured yet. However, the applied calibration factor gives better results than using solely the calibration factor for DME or ethanol.

Table 3: Weighting factors ionization cross sections of mole fractions of ethanol and dimethyl ether at specific gas temperatures separated by i^{2}PEPICO

	Gas temperature / K	fraction DME	fraction ethanol	fraction formic acid
OME_1	959	5.3 %	86.1 %	8.5 %
OME_3	866	7.7 %	60.0 %	32.3 %
OME_4	866	3.9 %	69.0 %	27.1 %
OME_5	866	2.6 %	54.1 %	43.3 %

Sun et al. [11] have stated a rate of production analysis for OME_3, where H-abstraction at the terminal C atom, followed by abstraction of three oxymethylene groups (-CH_2O) leads to C_2H_5O. This leads to the statement that less dimethyl ether is reformed from C_2H_5O and instead directly decompose to formaldehyde [11] for all OMEs. This assumption is supported by our study of laminar oxymethylene ether flames, where we have investigated an OME_1-doped hydrogen flame and pure OME flames: we could see that for the OME_1-doped hydrogen flame, the mole fraction of DME is increasing significantly due to the greater importance of the formation route: $CH_3OCH_2 + H_2 = CH_3OCH_3 + H$ [49]. Nevertheless, it can be stated that using calibration for pure DME results for the EI-MBMS results highly underestimates mole fractions profiles and ethanol has a strong impact on the quantification of C_2H_6O. To capture the main routes of ethanol formation, the mechanism by Kathrotia et al. [20] was used to calculate ethanol at the measured gas temperatures, used for the mole fraction calculations in Table 3 (see Fig. 12).

The main formation route seems thereby to be over $CH_2OH + CH_3 = C_2H_5OH$, followed by $CH_3CH_2O + H_2 = C_2H_5OH + H$. These two reactions also may be the starting point for further optimization. Formation routes via hydrocarbons are not playing a strong role at the chosen temperature for this mechanism. This point is underlined by the formation of hydrocarbons only at higher temperatures as seen in Fig. 7. Furthermore, Yu et al. have shown that the direct decomposition of OME_1 to formaldehyde and ethanol is highly unlikely to occur due to its high energy barrier [18]. Further experimental and model investigation have to be undertaken to clarify the contribution.

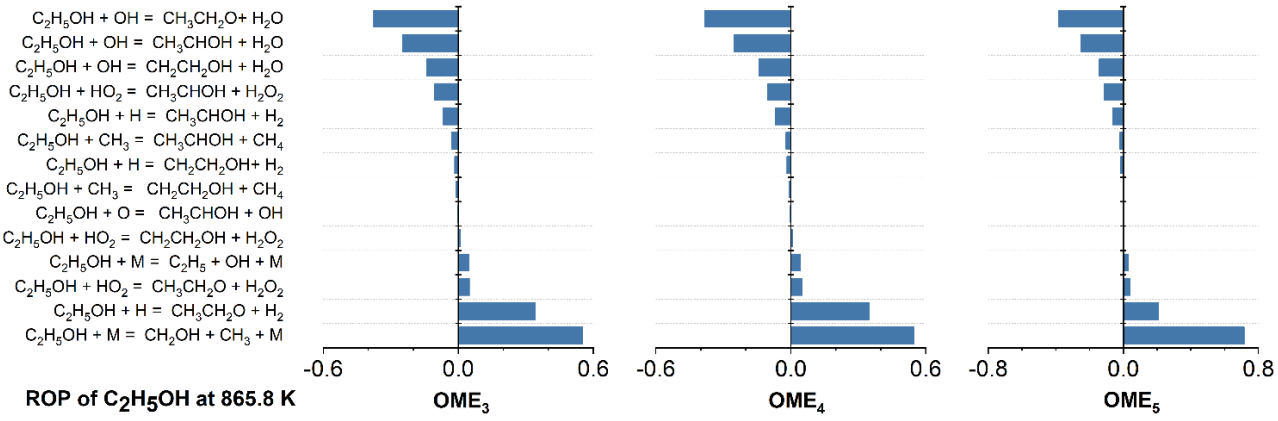

Fig. 12. Rate of production analysis (ROP) for ethanol in OME_{3-5} oxidation at measured gas temperature of 865.8 K using the mechanism by Kathrotia et al. [20].

Figure 13 shows a comparison of the models by Jacobs [8], Sun [11] and Kathrotia [20]: it can be seen that for formaldehyde and hydrocarbons all the models fit the experimental results quite well. For formaldehyde, the model by Jacobs et al. provides the best fit, while for the hydrocarbons, the model by Kathrotia fits better. DME and ethanol model results are combined in one graph. It can easily be seen that the mole fraction is thereby highly underestimated in all models.

The presented photoionization experiments providing explicit ethanol and DME quantification, provide a valuable source for further refinement of the presented kinetic models. However, expansion and improvement of these mechanism are beyond the scope of this study.

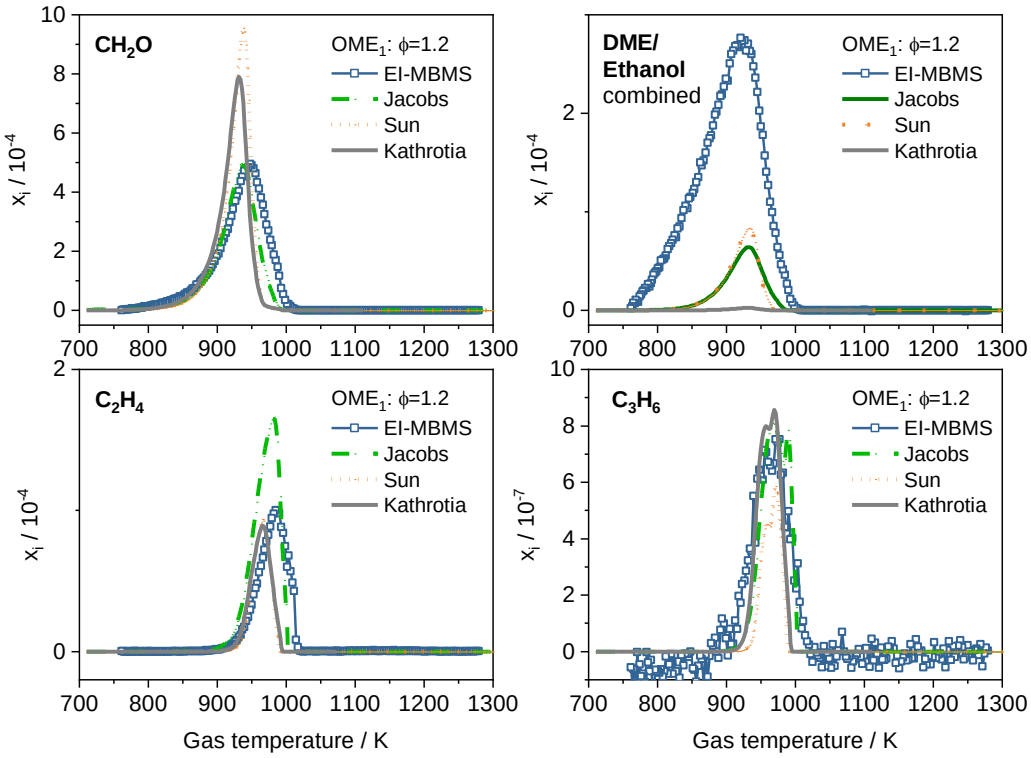

477

478 **Fig. 13:** Comparison of experimental results with models by Jacobs [8], Sun [11], and Kathrotia [20]

479 for OME_1, ϕ=1.2.

480 *Identification of m/z=44*

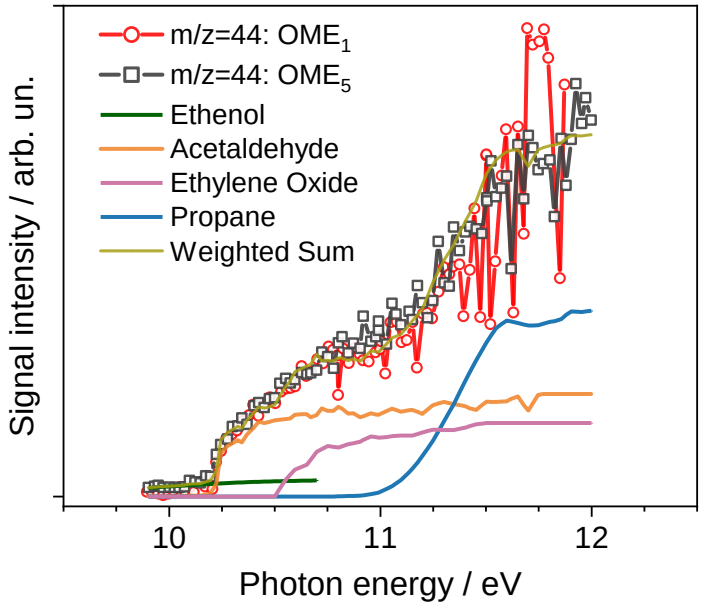

481

482 **Fig. 14:** Photoionization efficiency curves (PIE) of *m/z*=44 in comparison with literature spectra and

483 their weighted sum [47, 50-52].

Figure 14 displays the PIE curve of m/z=44 for OME_1 and OME_5 oxidation. Similar to *m/z*=46, also no TPES can be provided here, due to too low signal-to-noise ratios. Since OME_{3-5} show very similar oxidation behavior, only OME_5 results are shown in comparison to OME_1. The ionization thresholds of the C_2H_4O isomers ethenol and acetaldehyde are clearly identified in the measured PIE curves. Both are common intermediates in hydrocarbon oxidation [53]. Also, the third C_2H_4O isomer, ethylene oxide can be identified. Quantification shows that only 7.6 % of the measured signal is ethenol, while acetaldehyde is responsible for 49.5 % and ethylene oxide for 42.9 %. Calibration of C_2H_4O as acetaldehyde in the EI-MBMS analysis is therefore justifiable. Using the mechanism by Kathrotia et al., the main formation routes are thereby at the measured gas temperature: $CH_3CH_2O + M = CH_3CHO + H + M$ and $CH_3CHO + O_2 = CH_3CO + HO_2$. Kasper et al. have already shown for another oxygenated fuel, tetrahydrofuran in premixed flames that ethylene was detected as an intermediate using the PIE curve [52]. They claim that stabilization of $(CH_2)_2O$ to the cyclic ethylene oxide as a viable reaction even at high temperatures.

Furthermore, the strong increase of the PIE curve at 10.9 eV indicates the presence of propane as an intermediate in the OME oxidation even though it was not detected in the reactor measurements for $OME_{0–5}$.

Conclusions

This study presents the first systematic investigation of oxymethylene ethers with different number of oxymethylene ether groups (n=0-5). Dimethyl ether (DME) was treated as OME_0. Two complementary experimental setups were used to gain detailed information about the combustion process of longer OMEs. Isomer-selective intermediate identification was successfully performed at the i^2PEPICO reactor setup for $OME_{1,3-5}$. Furthermore, a high-temperature flow reactor was used to investigate the oxidation of the full series of OMEs by electron ionization molecular-beam mass spectrometry.

For all OMEs, oxygenated species are the dominating intermediates in the combustion process with formaldehyde showing the highest mole fractions. Highest oxygenated combustion intermediate is methyl formate for OME_{1-5}. No typical soot precursors, which are commonly observed during oxidation of hydrocarbons, are detected even for very fuel-rich conditions (ϕ=2.0). The flow reactor experiment

proves increased reactivity, i.e., a shift of the intermediate's peak temperature, for OMEs with a higher chain length. The observed species pool is nearly independent of the chain length of the OME.

For the isomer intermediates dimethyl ether and ethanol, quantitative separation was provided for $OME_{1,3\text{-}5}$. Noticeable, it was found that for all OMEs, the mole fraction of ethanol is overshooting those of DME. Similar behavior of OME_2 can be expected. As a consequence to this finding, ethanol is highly underestimated by present models and additional pathways or reaction rates have to be explored for OME combustion. Other intermediates, as acetaldehyde and methyl formate, could be confirmed and validated. The presented data is available and can be used for model development, further optimization of the reaction paths through its speciation and validation for OMEs with different chain lengths.

Acknowledgments

The authors acknowledge support from the Deutsche Forschungsgemeinschaft (DFG) under contract KA3871/3-2 and KO4786/2-2. Patrick Hemberger also acknowledges support from the Swiss Federal Office of Energy (SFOE) under contract SI/501269-01. Financial support is also acknowledged by the DLR project QSP Future Fuels. Experiments were performed at the VUV (X04DB) beamline of SLS of the Swiss Light Source, located at Paul Scherrer Institute. The authors gratefully thank Luka Debenjak and Patrick Ascher for technical assistance as well as Sophie Jürgens and Tobias Grein for analytical support.

References

[1] Burger J, Siegert M, Ströfer E, Hasse H. Poly(oxymethylene) dimethyl ethers as components of tailored diesel fuel: properties, synthesis and purification concepts. Fuel 2010; 89(11): 3315-9. https://doi.org/10.1016/j.fuel.2010.05.014

[2] Peukert S, Sela P, Nativel D, Herzler J, Fikri M, Schulz C. Direct measurement of high-temperature rate constants of the thermal decomposition of dimethoxymethane, a shock tube and modeling study. J Phys Chem A 2018; 122: 7559-72. https://doi.org/10.1021/acs.jpca.8b06558

[3] Gierlich CH, Beydoun K, Klankermayer J, Palkovits R. Challenges and opportunities in the production of oxymethylene dimethylether. Chem Ing Tech 2020; 92(1-2): 116-24. https://doi.org/10.1002/cite.201900187

[4] Kopp WA, Kröger LC, Döntgen M, Jacobs S, Burke U, Curran HJ, et al. Detailed kinetic modeling of dimethoxymethane. Part I: Ab initio thermochemistry and kinetics predictions for key reactions. Combust Flame 2018; 189: 433-42. https://doi.org/10.1016/j.combustflame.2017.07.037

[5] Li B, Li Y, Li H, Liu F, Wang Z, Wang J. Combustion and emission characteristics of diesel engine fueled with biodiesel/PODE blends. Appl Energy 2017; 206: 425-31. https://doi.org/https://doi.org/10.1016/j.apenergy.2017.08.206

[6] Marrodán L, Monge F, Millera Á, Bilbao R, U. M, Alzueta. Dimethoxymethane oxidation in a flow reactor. Combust Sci Technol 2016; 188: 719-29. https://doi.org/10.1080/00102202.2016.1138826

[7] Vermeire F, Carstensen H-H, Herbinet O, Battin-Leclerc F, Marin G, Geem KV. Experimental and modeling study of the pyrolysis and combustion of dimethoxymethane. Combust Flame 2018; 190: 270-83. https://doi.org/10.1016/j.combustflame.2017.12.001

[8] Jacobs S, Döntgen M, Alquaity ABS, Kopp WA, Kröger LC, Burke U, et al. Detailed kinetic modeling of dimethoxymethane. Part II: Experimental and theoretical study of the kinetics and reaction mechanism. Combust Flame 2019; 205: 522-33. https://doi.org/10.1016/j.combustflame.2018.12.026

[9] Sun W, Tao T, Lailliau M, Hansen N, Yang B, Dagaut P. Exploration of the oxidation chemistry of dimethoxymethane: Jet-stirred reactor experiments and kinetic modeling. Combust Flame 2018; 193: 491-501. https://doi.org/10.1016/j.combustflame.2018.04.008

[10] Sun W, Yang B, Hansen N, Moshammer K. The influence of dimethoxy methane (DMM)/dimethyl carbonate (DMC) addition on a premixed ethane/oxygen/argon flame. Proc Combust Inst 2017; 36(1): 449-57. https://doi.org/10.1016/j.proci.2016.06.145

[11] Sun W, Wang G, Li S, Zhang R, Yang B, Yang J, et al. Speciation and the laminar burning velocities of poly(oxymethylene) dimethyl ether 3 (POMDME3) flames: An experimental and modeling study. Proc Combust Inst 2017; 36(1): 1269-78. https://doi.org/10.1016/j.proci.2016.05.058

[12] He T, Wang Z, You X, Liu H, Wang Y, Li X, et al. A chemical kinetic mechanism for the low- and intermediate-temperature combustion of Polyoxymethylene Dimethyl Ether 3 (PODE3). Fuel 2018; 212: 223-6. https://doi.org/10.1016/j.fuel.2017.09.080

[13] Ngugi JM, Richter S, Braun-Unkhoff M, Naumann C, Riedel U. An investigation of fundamental combustion properties of the oxygenated fuels DME and OME1. *Proceedings of ASME Turbo Expo 2020: Turbomachinery Technical Conference and Exposition, Volume 3: Ceramics; Coal, Biomass, Hydrogen, and Alternative Fuels, Virtual, Online.* GT2020-14702.

[14] Ngugi JM, Richter S, Braun-Unkhoff M, Naumann C, Köhler M, Riedel U. A study on fundamental combustion properties of oxymethylene ether-2, OME2. *Proceedings of ASME Turbo Expo 2021 Turbomachinery Technical Conference and Exposition.* Virtual; 2021.

[15] Eckart S, Cai L, Fritsche C, vom Lehn F, Pitsch H, Krause H. Laminar burning velocities, CO, and NOx emissions of premixed polyoxymethylene dimethyl ether flames. Fuel 2021; 293: 120321. https://doi.org/10.1016/j.fuel.2021.120321

[16] Cai L, Jacobs S, Langer R, Lehn Fv, Heufer KA, Pitsch H. Auto-ignition of oxymethylene ethers (OME_n , n = 2–4) as promising synthetic e-fuels from renewable electricity: shock tube experiments and automatic mechanism generation. Fuel 2020; 264: 116711. https://doi.org/j.fuel.2019.116711

[17] Drost S, Schießl R, Werler M, Sommerer J, Maas U. Ignition delay times of polyoxymethylene dimethyl ether fuels (OME2 and OME3) and air: Measurements in a rapid compression machine. Fuel 2019; 258: 116070. https://doi.org/10.1016/j.fuel.2019.116070

[18] Yu T, Wu X, Zhou X, Bodi A, Hemberger P. Hydrogen migration as a potential driving force in the thermal decomposition of dimethoxymethane: New insights from pyrolysis imaging photoelectron photoion coincidence spectroscopy and computations. Combust Flame 2020; 222: 123-32. https://doi.org/10.1016/j.combustflame.2020.08.040

[19] Oßwald P, Zinsmeister J, Kathrotia T, Alves-Fortunato M, Burger V, Westhuizen Rvd, et al. Combustion kinetics of alternative jet fuels, Part-I: Experimental flow reactor study. Fuel 2021; 302: 120735. https://doi.org/10.1016/j.fuel.2021.120735

[20] Kathrotia T, Oßwald P, Naumann C, Richter S, Köhler M. Combustion kinetics of alternative jet fuels, Part-II: Reaction model for fuel surrogate. Fuel 2021; 302: 120736. https://doi.org/10.1016/j.fuel.2021.120736

[21] Oßwald P, Hemberger P, Bierkandt T, Akyildiz E, Köhler M, Bodi A, et al. In situ flame chemistry tracing by imaging photoelectron photoion coincidence spectroscopy. Rev Sci Instrum 2014; 85(2): 1-11. https://doi.org/10.1063/1.4861175

[22] Bierkandt T, Hemberger P, Oßwald P, Krüger D, Köhler M, Kasper T. Flame structure of laminar premixed anisole flames investigated by photoionization mass spectrometry and photoelectron spectroscopy. Proc Combust Inst 2019; 37: 1579-88. https://doi.org/10.1016/j.proci.2018.07.037

[23] Krüger D, Oßwald P, Köhler M, Hemberger P, Bierkandt T, Kasper T. The fate of the OH radical in molecular beam sampling experiments. Proc Combust Inst 2019; 37: 1563-70. https://doi.org/10.1016/j.proci.2018.05.041

[24] Oßwald P, Whitside R, Schäffer J, Köhler M. An experimental flow reactor study of the combustion kinetics of terpenoid jet fuel compounds: Farnesane, p-menthane and p-cymene. Fuel 2017; 187: 43-50. https://doi.org/10.1016/j.fuel.2016.09.035

[25] Bodi A, Johnson M, Gerber T, Gengeliczki Z, Sztaray B, Baer T. Imaging photoelectron photoion coincidence spectroscopy with velocity focusing electron optics. Rev Sci Instrum 2009; 80(3): 7. https://doi.org/10.1063/1.3082016

[26] Sztaray B, Voronova K, Torma KG, Covert KJ, Bodi A, Hemberger P, et al. CRF-PEPICO: Double velocity map imaging photoelectron photoion coincidence spectroscopy for reaction kinetics studies. J Chem Phys 2017; 147(1): 013944. https://doi.org/10.1063/1.4984304

[27] Bierkandt T, Oßwald P, Gaiser N, Krüger D, Köhler M, Hoener M, et al. Observation of low-temperature chemistry products in laminar premixed low-pressure flames by molecular-beam mass spectrometry. Int J Chem Kinet 2021; 53: 1063-81. https://doi.org/10.1002/kin.21503

[28] Oßwald P, Köhler M. An atmospheric pressure high-temperature laminar flow reactor for investigation of combustion and related gas phase reaction systems. Rev Sci Instrum 2015; 86: 1-12. https://doi.org/10.1063/1.4932608

[29] Bierkandt T, Hemberger P, Oßwald P, Köhler M, Kasper T. Insights in m-xylene decomposition under fuel-rich conditions by imaging photoelectron photoion coincidence spectroscopy. Proc Combust Inst 2017; 36(1): 1223-32. https://doi.org/10.1016/j.proci.2016.06.143

[30] Biordi JC. Molecular beam mass spectrometry for studying the fundamental chemistry of flames. Prog Energy Combust Sci 1977; 3(3): 151-73. https://doi.org/10.1016/0360-1285(77)90002-8

[31] Egolfopoulos FN, Hansen N, Ju Y, Kohse-Höinghaus K, Law CK, Qi F. Advances and challenges in laminar flame experiments and implications for combustion chemistry. Prog Energy Combust Sci 2014; 43: 36-67. https://doi.org/10.1016/j.pecs.2014.04.004

[32] Chemical Workbench. Version 4.1.19528. http://www.kintechlab.com/; 2017.

[33] Yang B, Wang J, Cool TA, Hansen N, Skeen S, Osborn DL. Absolute photoionization cross-sections of some combustion intermediates. Int J Mass Spectrom 2012; 309: 118-28. https://doi.org/10.1016/j.ijms.2011.09.006

[34] Wang Z, Liu H, Ma X, Wang J, Shuai S, D.Reitz R. Homogeneous charge compression ignition (HCCI) combustion of polyoxymethylene dimethyl ethers (PODE). Fuel 2016; 183: 206-13. https://doi.org/10.1016/j.fuel.2016.06.033

[35] Niu B, Jia M, Chang Y, Duan H, Dong X, Wang P. Construction of reduced oxidation mechanisms of polyoxymethylene dimethyl ethers (PODE1–6) with consistent structure using decoupling methodology and reaction rate rule. Combust Flame 2021; 232. https://doi.org/10.1016/j.combustflame.2021.111534

[36] Herrmann F, Jochim B, Oßwald P, Cai L, Pitsch H, Kohse-Höinghaus K. Experimental and numerical low-temperature oxidation study of ethanol and dimethyl ether. Combust Flame 2014; 161(2): 384-97. https://doi.org/10.1016/j.combustflame.2013.09.014

[37] Zhao P, Law CK. The role of global and detailed kinetics in the first-stage ignition delay in NTC-affected phenomena. Combust Flame 2013; 160(11): 2352-8. https://doi.org/10.1016/j.combustflame.2013.06.009

[38] Ren W, Dames E, Hyland D, Davidson DF, Hanson RK. Shock tube study of methanol, methyl formate pyrolysis: CH3OH and CO time-history measurements. Combust Flame 2013; 160(12): 2669-79. https://doi.org/10.1016/j.combustflame.2013.06.016

[39] Kohse-Höinghaus K, Oßwald P, Cool TA, Kasper T, Hansen N, Qi F, et al. Biofuel combustion chemistry: from ethanol to biodiesel. Angew Chem Int Ed Engl 2010; 49(21): 3572-97. https://doi.org/10.1002/anie.200905335

[40] Westbrook CK, Pitz WJ, Westmoreland PR, Dryer FL, Chaos M, Osswald P, et al. A detailed chemical kinetic reaction mechanism for oxidation of four small alkyl esters in laminar premixed flames. Proc Combust Inst 2009; 32(1): 221-8. https://doi.org/10.1016/j.proci.2008.06.106

[41] Taatjes CA, Welz O, Eskola AJ, Savee JD, Scheer AM, Shallcross DE, et al. Direct measurements of conformer-dependent reactivity o the criegee intermediate CH3CHOO. Science 2013; 340: 177-82. https://doi.org/10.1126/science.1234689

[42] Y. Nunes GM, N. J. Mason, D. Duflot, S. V. Hoffmann, J. Delwiche, M.-J. Hubin-Franskin,P. Limão-Vieira Electronic state spectroscopy of methyl formate probed by high resolution VUV

photoabsorption, He(I) photoelectron spectroscopy and ab initio calculations. Phys Chem Chem Phys 2010; (48): 15734-43 https://doi.org/10.1039/c0cp00051e

[43] Welz O, Burke MP, Antonov IO, Goldsmith CF, Savee JD, Osborn DL, et al. New insights into low-temperature oxidation of propane from synchrotron photoionization mass spectrometry and multiscale informatics modeling. J Phys Chem A 2015; 119(28): 7116-29. https://doi.org/10.1021/acs.jpca.5b01008

[44] Battin-Leclerc F. Detailed chemical kinetic models for the low-temperature combustion of hydrocarbons with application to gasoline and diesel fuel surrogates. Prog Energy Combust Sci 2008; 34: 440-98. https://doi.org/10.1016/j.pecs.2007.10.002

[45] Sarathy SM, Oßwald P, Hansen N, Kohse-Höinghaus K. Alcohol combustion chemistry. Prog Energy Combust Sci 2014; 44: 40-102. https://doi.org/10.1016/j.pecs.2014.04.003

[46] Esarte C, Abián M, Millera Á, Bilbao R, Alzueta MU. Gas and soot products formed in the pyrolysis of acetylene mixed with methanol, ethanol, isopropanol or n-butanol. Energy 2012; 43(1): 37-46. https://doi.org/10.1016/j.energy.2011.11.027

[47] Cool TA, McIlroy A, Qi F, Westmoreland PR, Poisson L, Peterka DS, et al. Photoionization mass spectrometer for studies of flame chemistry with a synchrotron light source. Rev Sci Instrum 2005; 76(9): 1-7. https://doi.org/10.1063/1.2010307

[48] Cool TA, Wang J, Nakajima K, Taatjes CA, Mcllroy A. Photoionization cross sections for reaction intermediates in hydrocarbon combustion. Int J Mass Spectrom 2005; 247(1-3): 18-27. https://doi.org/10.1016/j.ijms.2005.08.018

[49] Gaiser N, Zhang H, Bierkandt T, Schmitt S, Zinsmeister J, Kathrotia T, et al. Investigation of the combustion chemistry in laminar, low-pressure oxymethylene ether flames (OME0-4). Combust Flame 2021; under review.

[50] Cool TA, Nakajima K, Mostefaoui TA. Selective detection of isomers with photoionization mass spectrometry for studies of hydrocarbon flame chemistry. J Chem Phys 2003; 119(16): 8356. https://doi.org/10.1063/1.1611173

690 [51] Liu F, Qi F, Gao H, Sheng L, Zhang Y. A vacuum ultraviolet photoionization mass
691 spectrometric study of ethylene oxide in the photon energy region of 10-40 eV. J Phys Chem
692 A 1999; 103(41): 8179–86. https://doi.org/10.1021/jp984626b
693 [52] Kasper T, Lucassen A, Jasper AW, Li W, Westmoreland PR, Kohse-Höinghaus K, et al.
694 Identification of tetrahydrofuran reaction pathways in premixed flames. Z Phys Chem 2011;
695 225(11-12): 1237-70. https://doi.org/10.1524/zpch.2011.0163
696 [53] Taatjes CA, Hansen N, McIlroy A, Miller JA, Senosiain JP, Klippenstein SJ, et al. Enols are
697 common intermediates in hydrocarbon oxidation. Science 2005; 308(5730): 1887-9.
698 https://doi.org/10.1126/science.1112532

699